IOPscience iopscience.iop.org

Home Search Collections Journals About Contact us My IOPscience

Conduction band structure and electron mobility in uniaxially strained Si via externally applied strain in nanomembranes

This article has been downloaded from IOPscience. Please scroll down to see the full text article.

2011 J. Phys. D: Appl. Phys. 44 325107

(http://iopscience.iop.org/0022-3727/44/32/325107)

View the table of contents for this issue, or go to the journal homepage for more

Download details:
IP Address: 155.98.5.152
The article was downloaded on 26/02/2012 at 04:11

Please note that terms and conditions apply.

IOP Publishing Journal of Physics D: Applied Physics
J. Phys. D: Appl. Phys. **44** (2011) 325107 (8pp) doi:10.1088/0022-3727/44/32/325107

Conduction band structure and electron mobility in uniaxially strained Si via externally applied strain in nanomembranes

Feng Chen[1,2], Chanan Euaruksakul[2,4], Zheng Liu[3,5], F J Himpsel[2], Feng Liu[3] and Max G Lagally[2]

[1] Xi'an Jiaotong University, Xi'an, Shaanxi 710049, People's Republic of China
[2] University of Wisconsin-Madison, Madison, WI 53706, USA
[3] University of Utah, Salt Lake City, UT 84112, USA

E-mail: lagally@engr.wisc.edu

Received 7 April 2011, in final form 28 June 2011
Published 27 July 2011
Online at stacks.iop.org/JPhysD/44/325107

Abstract
Strain changes the band structure of semiconductors. We use x-ray absorption spectroscopy to study the change in the density of conduction band (CB) states when silicon is uniaxially strained along the [1 0 0] and [1 1 0] directions. High stress can be applied to silicon nanomembranes, because their thinness allows high levels of strain without fracture. Strain-induced changes in both the sixfold degenerate Δ valleys and the eightfold degenerate L valleys are determined quantitatively. The uniaxial deformation potentials of both Δ and L valleys are directly extracted using a strain tensor appropriate to the boundary conditions, i.e., confinement in the plane in the direction orthogonal to the straining direction, which correspond to those of strained CMOS in commercial applications. The experimentally determined deformation potentials match the theoretical predictions well. We predict electron mobility enhancement created by strain-induced CB modifications.

(Some figures in this article are in colour only in the electronic version)

1. Introduction

In the search for routes to improve the performance of Si-based electronic devices, strain has been introduced into Si technology as a means of enhancing charge carrier mobility. Utilizing uniaxial strain in modern low-dimensional electronic devices is now common, and uniaxially strained Si has emerged as the next scaling vector in logic technologies [1].

Strain in general increases the charge carrier mobility in Si(0 0 1). In-plane biaxial tensile (out-of-plane uniaxial compressive) strain removes the degeneracy in the four in-plane valleys (Δ_4) and the two out-of-plane valleys (Δ_2) of the conduction band minimum (CBM) by splitting them in energy [2]. The lower energy of the Δ_2 valleys means that they are preferentially occupied by electrons. The electron mobility is enhanced via increased population in this Δ_2 conduction band (CB) valley. Simulations by others have investigated the effect of biaxial strain on CB and valence band (VB) structures [3], including changes in the effective mass [3, 4], to explain how the mobility of electrons and holes changes. The electron mobility in biaxially strained Si (0 0 1) improves partially via a higher fraction of in-plane electrons with lower effective masses (m^*) and a lower fraction of out-of-plane electrons with higher effective mass. The electron redistribution and average effective-mass reduction by strain are only part of the mobility enhancement [5]. Electron scattering is also reduced by the CBM splitting, because of the lower rate of inter-valley phonon scattering between Δ_2 and Δ_4 valleys [4].

Uniaxial strain enhances transport properties for both electrons and holes. Uniaxial strain provides enhancement of the electron mobility that is as large as or larger than that for biaxial strain. For holes, uniaxial strain provides

[4] Current address: Synchrotron Light Research Institute, Nakhon Ratchasima 30000, Thailand.
[5] Current address: Institute for Advanced Study, Tsinghua University, Beijing 10084, People's Republic of China.

 © 2011 IOP Publishing Ltd Printed in the UK & the USA

a low channel-direction in-plane conductivity mass, a large out-of-plane confinement mass and a high in-plane density of states of the ground state hole sub-band. All these band changes are important and allow an extremely significant $\sim 4\times$ enhancement in the hole mobility [6]. Thus, in MOSFET design it is common to grow SiGe alloy from the side in pFETs to compress the Si channel (SiGe having a larger lattice constant than Si) to boost the hole mobility, and to grow a silicon nitride capping film for nFETs to create tensile strain in the channel to enhance the electron mobility [7, 8].

We use x-ray absorption spectroscopy (XAS) with synchrotron radiation to determine the influence of uniaxial tensile strain in Si(0 0 1) on the CB structure in a configuration that mimics industrial practice, in that the structure in the direction in-plane but orthogonal to the strain direction is confined [9–12], but in the direction out of plane the lattice can contract in response to the uniaxial tensile stress. The advantage of direct measurements is that there are no parameters that require assumptions. We use Si(0 0 1) nanomembranes (SiNM) less than 100 nm thick on a host that is flexible. The thinness of the membrane relative to the host allows us to introduce a considerable strain in the Si. From the strain dependence of the XAS spectra, we extract the sub-band splitting for Δ and L valleys and use the values of sub-band splitting to estimate changes in mobility with strain.

It is important to note that the boundary conditions under which strain is applied significantly influence the interpretation of the measurements. In our past work using XAS on strained-Si nanomembranes, we introduced in-plane biaxial strain via growth: the boundary conditions laterally are 'free', and by Poisson's ratio we have uniaxial compressive strain normal to the nanomembrane [13]. Clearly the boundary conditions for the industrial approaches described above imply confinement of the lattice in lateral directions orthogonal to the uniaxial-strain direction [8, 11, 12]. This means of introducing strain is different from putting uniaxial stress on a freestanding bar. When we apply a tensile force on both ends of a square bar, in the directions perpendicular to the stress direction the dimensions shrink following Poisson's ratio [14]. In the current measurements we therefore modify the strain tensor to be appropriate for these constraints.

Prior experimental studies involving uniaxial strain in Si(0 0 1) were indirect in the sense that they measured charge transport as a function of strain [15–19], and from these measurements deduced deformation potentials using a number of assumptions, including the nature of the strain tensor. There are two ways to fabricate a FET device and measure the mobility. One is to build the FET on a bulk-Si wafer and then bend the wafer. In this configuration, the lattice is unconfined in all directions; therefore free-boundary conditions are appropriate and the proper strain tensor has no confined component [20]. However, when the in-plane orthogonal dimensions are confined, such as in a SiN-capped tensilely strained channel, the interpretation requires a modification of the strain tensor [12]. Our experiments require a modified stress tensor.

Theoretical values of deformation potentials for different (but not all) features of the band structure of Si have existed for some time. They are obtained with first-principles and pseudopotential methods [3, 4, 21–23]. In our past work [2, 13] on biaxial strain, the extracted deformation potentials fit theory well, as described later. We will show that deformation potentials extracted for uniaxial strain with a proper strain tensor also fit theory well. From that agreement we can be confident in estimating mobility changes with strain.

Specifically, in the current measurements, when we strain a (0 0 1) SiNM uniaxially along the [1 0 0] direction, the in-plane [0 1 0] direction is confined by the substrate on which the NM is bonded, but the out-of-plane [0 0 1] direction is free to move. Because NM transfer allows control of the orientation of the SiNM, we can also strain the membrane along [1 1 0] with the $[\bar{1}\,1\,0]$ direction confined and the out-of-plane direction ([0 0 1]) free to move. We measure the changing positions of the Δ, L_1 and L_3 valleys under these conditions, for strains as high as 1.5%, values that can be achieved without damage to the NM.

We find that, under [1 0 0] uniaxial strain with the lattice confined in the in-plane orthogonal to the strain direction, the Δ_6 valley splits into three sets of twofold Δ_2 valleys, but that there is no effect on L valleys. For [1 1 0] uniaxial strain, the Δ_6 valley splits into Δ_2 and Δ_4 valleys, and L_1 and L_3 valleys both split into two sets of fourfold degenerate L_1 and L_3 valleys. The deformation potentials for Δ and L_1 valleys extracted from the data match theoretical predictions [24–26]. The L_3 valley deformation potential is determined for the first time. We extract the mobility enhancement for [1 0 0] uniaxial strain; it is higher compared with that for biaxially strained Si(0 0 1) and higher than predictions using a strain tensor that has not been modified for the confined-lattice boundary conditions.

2. Experimental

Because they are strainable to a much greater degree than bulk materials, we use silicon nanomembranes, very thin, single-crystal sheets that are flexible, conformable, and readily transferable and bondable. Fabrication of such membranes has been described elsewhere [27–29]. We transfer and bond the SiNM to a flexible host substrate that is considerably thicker than the NM, and is ultrahigh-vacuum compatible, here a molybdenum (Mo) sheet. Mo additionally can survive hydrofluoric acid (HF), important as one step of processing involves etching in HF. We use wet transfer of a SiNM released from silicon-on-insulator (SOI) by selectively etching the buried oxide (BOX) with HF, which is then slowly replaced by deionized water. We pick the SiNM up from the deionized water, with a pre-polished Mo foil ($\sim$130 μm thick) and bond it to the Mo via rapid thermal annealing under nitrogen gas ambient at a temperature of 350 °C for 5 min. To deform the host substrate in the appropriate manner, a four-point load is applied [30], as shown in figure 1(*a*). The loading jig introduces uniaxial elastic strain in the SiNM. Because its thickness is only of the order of tens of nanometres, the SiNM can be highly strained without cracking or generating dislocations, something that is easy to see from simple strain balance and critical-thickness considerations [27–29]. As the Mo substrate only deforms along the bending direction, the

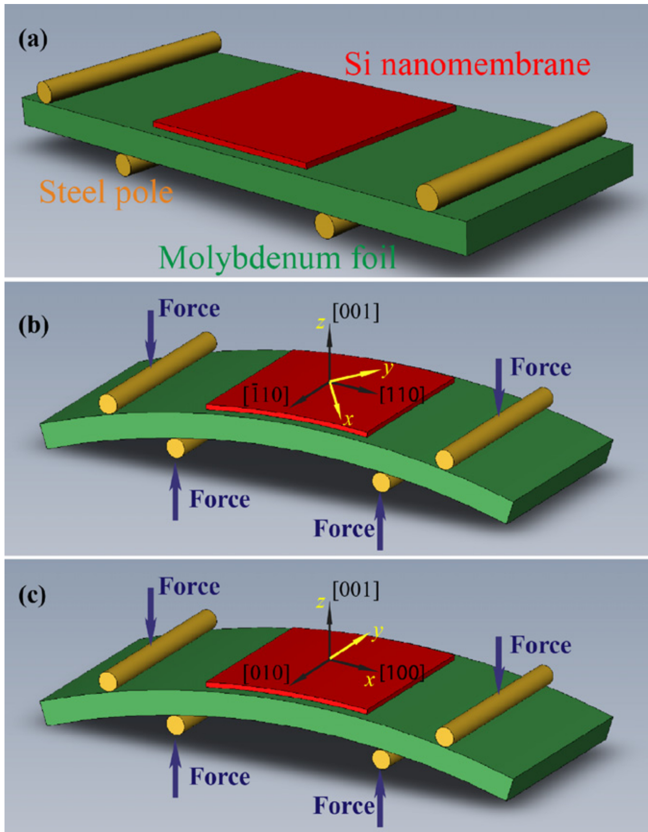

Figure 1. Schematic diagram of the four-point bending technique to generate uniaxial strain in Si(0 0 1) nanomembranes. (*a*) Without strain. (*b*) and (*c*) With uniaxial strain along [1 1 0] and [1 0 0], respectively. The coordinates x, y and z are defined as the [1 0 0], [0 1 0] and [0 0 1] directions.

SiNM will stretch along that direction and shrink in the out-of-plane direction, without change in the in-plane direction orthogonal to the bending direction. Because the membrane is so thin compared with Mo substrate, its change in radius of curvature is negligible and strain induced by membrane bending can be ignored. The deformation of the Mo substrate is plastic and thus irreversible, so we cannot cycle the system but must start with a new substrate once we have reached the maximum strain for a given membrane.

The degree of strain in a SiNM can be well controlled by the deformation of the Mo substrate, and can be measured using ultraviolet (UV) Raman spectroscopy [31]. Because the penetration depth of UV light (325 nm in this experiment) is only 8–10 nm, the Raman measurement is easily performed on thin Si sheets. In-plane tensile strain moves the Si Raman line to lower wavenumber, while compressive strain has the opposite effect. In this experiment, we used a 4 × 4 matrix point-selection method on a large area ($1 \times 1\,\mathrm{mm}^2$) in each sample. We found that the strain variation was in the range of ±0.2%. Strains mentioned in this paper all indicate the strain along the stressing direction. Strains were also confirmed with a sensitive strain gauge.

We use XAS with total-electron-yield detection to characterize the CB structure modification, including the Δ, L_1 and L_3 valleys. Because XAS in this mode is very sensitive to the near-surface region, we cleaned the surface to remove the native oxide by dipping all samples into HF just prior to transfer into the ultrahigh-vacuum chamber. The hydrogen-terminated surface can prevent oxidation for hours [32]; the transfer of the sample into vacuum occurs in less than 5 min. The Variable-Line-Spacing Plane Grating Monochromator beam line at the University of Wisconsin Synchrotron Radiation Center provided photons with 10 meV energy resolution in the energy range of interest (99.5–106 eV). An unstrained Si wafer with a hydrogen-terminated surface was used as reference. Before and after each sample was measured, we took reference data three times to eliminate any photon energy drift. The spectra were normalized by the incident photon intensity, which was obtained from the photocurrent of a gold mesh in front of the sample, and averaged to improve the signal-to-noise ratio. Derivatives of the spectra were used to determine the onset of the absorption at each valley, which appears as a peak in the derivative [2]. Representative spectra from an Si wafer and two NMs with different uniaxial strains are shown in figure 2(*a*). Figure 2(*b*) shows the electronic band structure of silicon schematically.

3. Results and discussion

XAS has proven to be effective for measuring the CB structure in semiconductors [13], with most attention paid to the absorption edge, which is the position of the CBM relative to the core level [33]. In recent work, we used XAS to measure the influence of strain on the CB structure in biaxially strained Si(0 0 1) NMs [2, 13]. We characterized not only the splitting of the CBM valley and its shift with strain but also the shifts of higher-energy valleys with increasing strain.

When uniaxial strain is created along the [1 1 0] direction in a Si(0 0 1)NM by bending the host substrate, the in-plane [$\bar{1}$ 1 0] direction (orthogonal to the strain direction) will be confined by the substrate, but in the out-of-plane [0 0 1] direction the crystal is free to move (figure 1(*b*)). As expected, we find no strain in the confined direction, which we confirmed using a sensitive strain gauge. The strain tensor for [1 1 0] uniaxial strain in the Si (0 0 1) nanomembrane can be expressed as

$$\overleftrightarrow{\varepsilon}_{[1\,1\,0]} = \begin{pmatrix} \frac{1}{2}\varepsilon_\parallel & \frac{1}{2}\varepsilon_\parallel & 0 \\ \frac{1}{2}\varepsilon_\parallel & \frac{1}{2}\varepsilon_\parallel & 0 \\ 0 & 0 & \varepsilon_\perp \end{pmatrix} = \begin{pmatrix} \frac{1}{2}\varepsilon & \frac{1}{2}\varepsilon & 0 \\ \frac{1}{2}\varepsilon & \frac{1}{2}\varepsilon & 0 \\ 0 & 0 & -\dfrac{c_{12}}{c_{11}}\varepsilon \end{pmatrix}, \quad (1)$$

where $\varepsilon_\parallel$ is the strain along [1 1 0], $\varepsilon_\perp$ is the strain normal to the surface, along [0 0 1], and ε is measured in this experiment. The strain tensor for uniaxial strain along [1 0 0] (figure 1(*c*)) can be expressed as

$$\overleftrightarrow{\varepsilon}_{[1\,0\,0]} = \begin{pmatrix} \varepsilon_\parallel & 0 & 0 \\ 0 & 0 & 0 \\ 0 & 0 & \varepsilon_\perp \end{pmatrix} = \begin{pmatrix} \varepsilon & 0 & 0 \\ 0 & 0 & 0 \\ 0 & 0 & -\dfrac{c_{12}}{c_{11}}\varepsilon \end{pmatrix}, \quad (2)$$

where $\varepsilon_\parallel$ is the strain along [1 0 0] and $\varepsilon_\perp$ is the strain normal to the surface (along [0 0 1]).

Strain lowers the crystal symmetry and thus lifts the symmetry-determined band degeneracies according to the

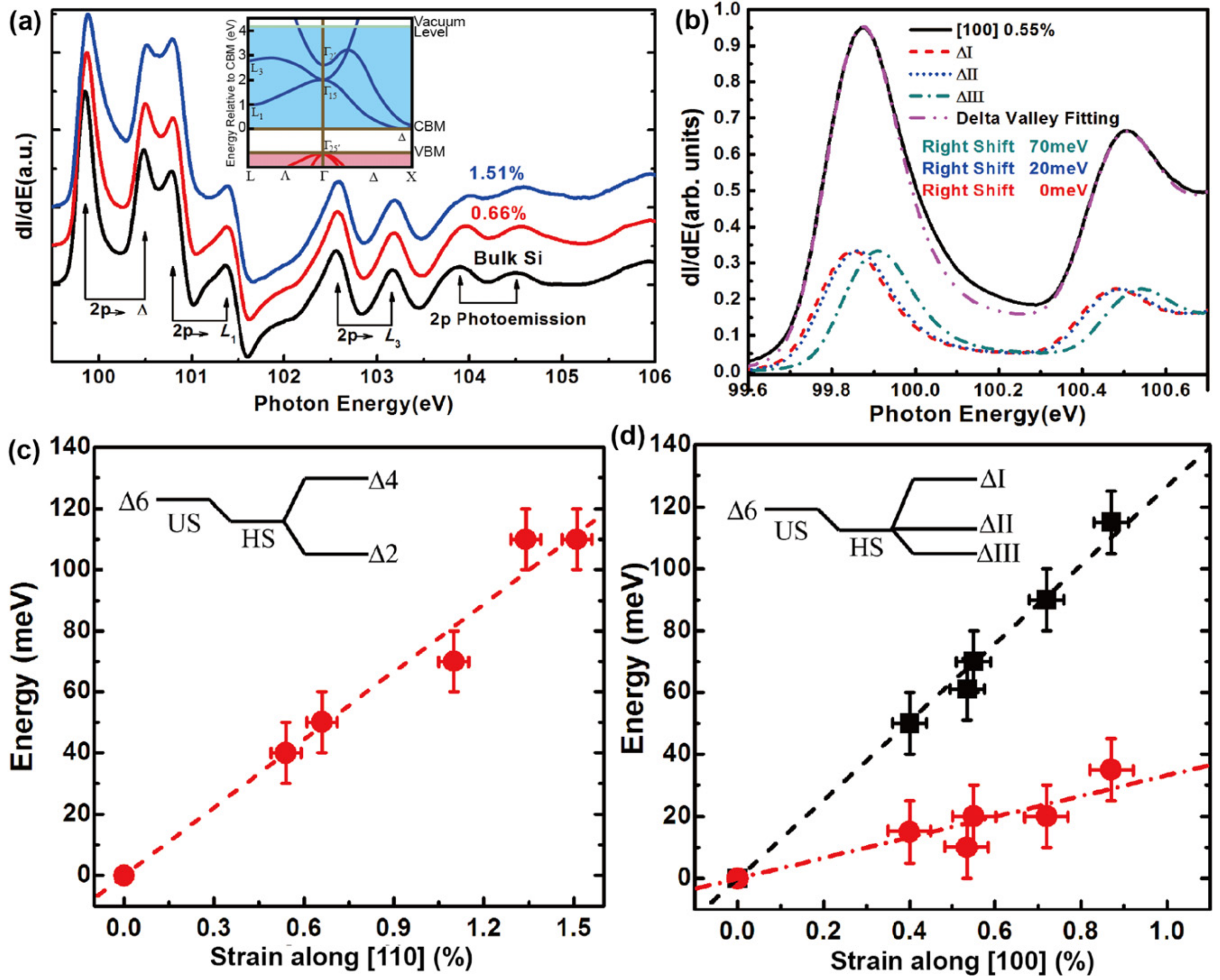

Figure 2. Results from XAS for uniaxial strain along [1 1 0] and [1 0 0]. (*a*) First derivative of XAS spectra for fully relaxed bulk Si and from a Si(0 0 1) nanomembrane under [1 1 0] uniaxial tensile strain, for strains of 0.66% and 1.51%. Peaks correspond to optical transitions from the Si 2p core level to CB valleys. They come in pairs because of the spin–orbit splitting of the 2p level. The inset in (*a*) shows the Si band structure including the sixfold degenerate CBM Δ and the eightfold degenerate L_1 and L_3 valleys. (*b*) Example of a fit to determine Δ valley splitting for 0.55% strain along [1 0 0], corresponding to a pair of data points in (*d*). (*c*) Splitting of the Δ valley between Δ_2 to Δ_4 as a function of uniaxial strain along [1 1 0] with structure confined in the [1 $\bar{1}$ 0] direction. (*d*) Splitting of the Δ valley for uniaxial strain along [1 0 0] with [0 1 0] confined. Squares and circles are for the splitting ΔI–ΔIII and ΔII–ΔIII. The insets in (*c*) and (*d*) show the energy shifts from unstrained (US) to hydrostatic strain (HS) and the splittings induced by uniaxial strain. Dashed lines are guides to the eye.

linear deformation potential theory developed by Herring and Vogt [34]. The shift of an individual CB valley (distinguished by its direction in momentum space among the degenerate valleys) follows the equation:

$$\Delta E^{ijk} = [\Xi_d \overleftrightarrow{1} + \Xi_u(\hat{a}_{ijk} \otimes \hat{a}_{ijk})] : \overleftrightarrow{\varepsilon}, \tag{3}$$

where ΔE^{ijk} is the energy shift of an individual CB valley sitting in the $\langle ijk \rangle$ direction, Ξ_d is the dilation deformation potential, Ξ_u is the uniaxial deformation potential, $\hat{a}_{ijk}$ is a unit vector along the direction of the valley *ijk*, $\overleftrightarrow{1}$ is a unit tensor and $\overleftrightarrow{\varepsilon}$ is the strain tensor. $\hat{a}_{ijk} \otimes \hat{a}_{ijk}$ denotes a self-dyadic product of $\hat{a}_{ijk}$. Uniaxial strain leads to a splitting of CB minima that are degenerate in the absence of strain. According to equations (1)–(3), for uniaxial strain along [1 1 0], the sixfold degenerate Δ valley evolves to two sets of sub-bands, Δ_2 and Δ_4. [1 0 0] uniaxial strain splits the sixfold degenerate Δ valley into three sets of Δ_2 sub-bands, ΔI, ΔII, and ΔIII.

According to deformation potential theory developed by Bardeen and Shockley and equations (1)–(3) [35], the splitting between Δ_2 and Δ_4 for uniaxial strain along [1 1 0] is

$$\Delta E_{\Delta}^{[1\,1\,0]} = \Delta E_{\Delta_4}^{1\,0\,0,\bar{1}\,0\,0,0\,1\,0,0\,\bar{1}\,0} - \Delta E_{\Delta_2}^{0\,0\,1,0\,0\,\bar{1}} = \left(\frac{1}{2} + \frac{c_{12}}{c_{11}}\right) \Xi_u^{\Delta} \cdot \varepsilon, \tag{4}$$

where ε is the uniaxial strain, Ξ_u^{Δ} is the uniaxial deformation potential, and c_{11} and c_{12} are the compliance coefficients of Si [36].

Uniaxial strain along [1 0 0] splits the CBM differently compared with uniaxial strain along [1 1 0] or (0 0 1) biaxial strain. Instead of two sets of sub-bands, uniaxial strain along [1 0 0] with [0 1 0] confined will create three sets of sub-bands

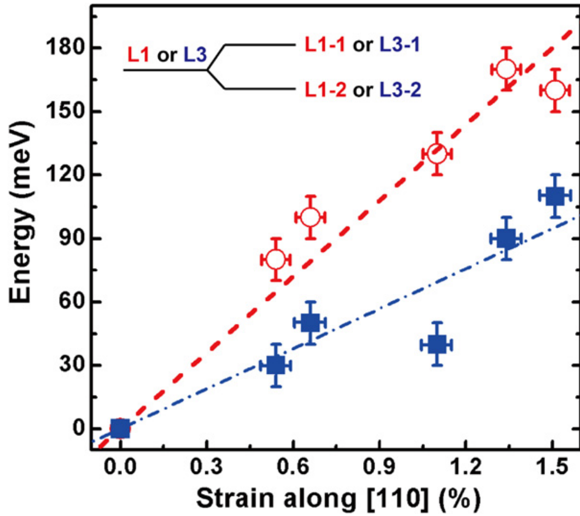

Figure 3. Influence of uniaxial strain along [1 1 0] on the L valleys along ⟨1 1 1⟩. The open circles are data for the L_1 valley splitting and the solid squares for the L_3 valley. The lines are guides to the eye.

with each set doubly degenerate, marked as ΔI, ΔII, and ΔIII. The energy splitting between each pair is

$$\Delta E_{\Delta \mathrm{I}} - \Delta E_{\Delta \mathrm{III}} = \Delta E_{\Delta}^{100,\bar{1}00} - \Delta E_{\Delta}^{001,00\bar{1}} = \left(1 + \frac{c_{12}}{c_{11}}\right) \Xi_{\mathrm{u}}^{\Delta} \cdot \varepsilon, \quad (5)$$

$$\Delta E_{\Delta \mathrm{II}} - \Delta E_{\Delta \mathrm{III}} = \Delta E_{\Delta}^{010,0\bar{1}0} - \Delta E_{\Delta}^{001,00\bar{1}} = \frac{c_{12}}{c_{11}} \cdot \Xi_{\mathrm{u}}^{\Delta} \cdot \varepsilon. \quad (6)$$

To fit the experimental spectrum we use three equal-weight peaks with the shape of the Si bulk spectrum, the procedure described earlier. The fit to the [1 0 0] 0.55% strain data is shown in figure 2(*b*).

When uniaxial strain is applied along the [1 1 0] direction, the degeneracy of the eightfold L valley along ⟨1 1 1⟩ will be lifted to two sets of fourfold degenerate valleys. We fit data according to the instruction in [13] to determine the magnitude of the splitting of Δ and L valleys. For uniaxial strain along [1 0 0] the spectra for the Δ valleys are fitted by three 1/3-intensity bulk-Si reference spectra. For uniaxial strain along [1 1 0] the spectra for the Δ valleys are fitted by 1/3 and 2/3-intensity bulk reference spectra, while for the L valleys, they are fit by 1/2-intensity bulk reference spectra [4, 24]. Figures 2(*b*) and (*c*) show the experimental results for the Δ valley splitting for uniaxial strain along [1 1 0] and [1 0 0]. The insets in these figures show the splittings schematically. L_1 and L_3 valley splitting as a function of strain along [1 1 0] is shown in figure 3.

The eightfold degenerate L valleys (L_1 and L_3) of Si, along the ⟨1 1 1⟩ directions, will be affected if the coincident symmetric structure changes with strain. Uniaxial tensile strain along [1 0 0] with [0 1 0] confined has the same effect on all ⟨1 1 1⟩ directions, thus, no degeneracy will be lifted. However, [1 1 0] uniaxial strain (with [1 $\bar{1}$ 0] confined) will lift the degeneracy of the L_1 valley from eightfold to two sets of fourfold degenerate sub-bands: L_1-1 and L_1-2. The L_3 valley also splits. The splitting between L_1-1 and L_1-2 is

$$\Delta E_{\mathrm{L}_1} = \Delta E_{\mathrm{L}_1}^{111,\bar{1}\bar{1}\bar{1},11\bar{1},\bar{1}\bar{1}1} - \Delta E_{\mathrm{L}_1}^{1\bar{1}1,\bar{1}1\bar{1},1\bar{1}\bar{1},\bar{1}11} = \tfrac{2}{3}\,\Xi_{\mathrm{u}}^{\mathrm{L}_1} \cdot \varepsilon, \quad (7)$$

where $\Xi_{\mathrm{u}}^{\mathrm{L}_1}$ is the uniaxial deformation potential of the L_1 valley. For the L_3 valley, the splitting can be expressed as

$$\Delta E_{\mathrm{L}_3} = \Delta E_{\mathrm{L}_3}^{111,\bar{1}\bar{1}\bar{1},11\bar{1},\bar{1}\bar{1}1} - \Delta E_{\mathrm{L}_3}^{1\bar{1}1,\bar{1}1\bar{1},1\bar{1}\bar{1},\bar{1}11} = \tfrac{2}{3}\,\Xi_{\mathrm{u}}^{\mathrm{L}_3} \cdot \varepsilon, \quad (8)$$

where $\Xi_{\mathrm{u}}^{\mathrm{L}_3}$ is defined as the uniaxial deformation potential of the L_3 valley.

From these theoretical expressions, the deformation potentials of all valleys can be extracted, as summarized in table 1. The agreement of experimentally determined deformation potential constants of the Δ and L_1 valleys with theoretical predictions indicates the strain tensors modified to account for the lattice confinement along the orthogonal in-plane direction are appropriate. If we use the unmodified strain tensors (the ones appropriate for the free boundary conditions), strain along [0 0 1] will split the Δ valley to fourfold and twofold degeneracy. Efforts to fit the XAS data with this degeneracy do not produce as good fits as three sets of twofold degenerate valleys. Also the deformation potentials will deviate from the theoretical prediction. We therefore have confidence to extract the uniaxial deformation potential of L_3 valley, $\Xi_{\mathrm{u}}^{\mathrm{L}_3}$, for which there is no prior calculation or measurement.

Using the valley splitting data in figure 2, we are able to predict semi-quantitatively how uniaxial strain will influence the electron mobility. In general, the influence of strain on electron mobility has two origins: valley splitting and valley deformation. On the one hand, when strain breaks the crystal symmetry, the degeneracy of the six originally equivalent CBM valleys along Δ directions will be partially removed, leading to valley splitting. It forces electrons to re-populate the six valleys and, in combination with the anisotropy of these valleys between longitudinal and transverse directions, it influences the overall electron mobility. Meanwhile, the valley splitting will also influence the inter-valley scattering intensity. On the other hand, strain may influence the valley shapes and in turn changes the effective mass, the density of states, and the intra-valley scattering intensity.

According to previous density functional theory (DFT) calculations on biaxial-strain effects and pseudopotential calculations on uniaxial-strain effects [4, 22, 37], within the range of strain from 2% compressive to 2% tensile, the dominant effect on mobility tuning is valley splitting, while the valley shapes remain almost unchanged. Therefore, it is reasonable to assume that the effective-mass tensor of each valley is constant and to treat the electron mobility as a function of valley splitting only. We calculate the electron mobility within the relaxation time approximation as [37]

$$\mu_{xx} = \sum\nolimits_{\alpha} \gamma_{\alpha} \frac{e\langle \tau^{\alpha} \rangle}{m_x^{\alpha}}, \quad (9)$$

where α runs over all the six Δ valleys, γ_α are the electron population ratios for each of the valleys and $\langle \tau^{\alpha} \rangle$ and m_x^{α} are

Table 1. Comparison of deformation potentials extracted from XAS data of the valley splitting in Si(0 0 1) for uniaxial strain along the [1 1 0] and [1 0 0] directions with theory and our earlier results for in-plane biaxial strain [2, 13] and one other direct measurement [40]. Different theory values from the same reference are obtained using different calculation methods. No theory or experiment exists for $\Xi_u^{L_3}$. The Ξ_u^{Δ} values for uniaxial strain along [1 1 0] and along [1 0 0] should be and are, within error, the same. All quantities are in eV.

	Theory	Uniaxial strain	Biaxial strain	This work
Ξ_u^{Δ}	9.0[a], 8.79[b], 9.01[b],	8.6 ± 0.4[c]	8.3[d]	9.1 ± 0.2[e], 8.5 ± 0.6[f]
$\Xi_u^{L_1}$	15.9[a], 13.85[b], 15.1[b], 16.14[g], 18.0[h]		16.5[d]	18.1 ± 0.2[e]
$\Xi_u^{L_3}$				9.5 ± 0.9[e]

[a] Reference [25].
[b] Reference [26], using two methods.
[c] Reference [40], from low-temperature (77 K) indirect-exciton spectrum.
[d] Reference [13], from XAS data;
[e] with uniaxial strain along [1 1 0].
[f] with uniaxial strain along [1 0 0].
[g] Reference [23].
[h] Reference [22].

the average relaxation times and effective masses along the given direction.

The average relaxation time $\langle\tau^{\alpha}\rangle$ is defined to be the inverse of the thermal-averaged scattering rates as equation (7) in [4] and is obtained in our methodology by simple numerical integration. The individual scattering rates for intra-valley and inter-valley electron–phonon scattering are calculated following (3.47) and (3.74) in [38] under an elastic, energy-equipartition and isotropic approximation. The model has given good results for electron mobility of silicon under strain [22]. The related parameters in these formulae are chosen to be exactly the same as in [4]. Impurity scattering and electron–electron scattering are neglected.

We point out that the calculated mobility greatly depends on the parameters we use, e.g., average deformation potential, phonon energy, etc. We use the deformation potentials determined from XAS experiments. They agree for biaxial strain and uniaxial strain (table 1). The uncertainty in phonon energy becomes less important when the same set of parameters is used throughout our calculations.

Because we focus on the effect of valley splitting on electron mobility, our calculation can be used for both uniaxial and biaxial strain. To that end, before calculating the mobility in our scenario, we applied the above method to calculate the in-plane and out-of-plane electron mobilities under two different biaxial-strain conditions, as recently studied experimentally in [13]. Because we are able to reproduce the mobility of previous work [4], we believe that our calculation is reliable. The calculated mobility is shown in figure 4. We plot the in-plane mobility along the strain direction (longitudinal) and orthogonal to the strain direction (transverse), respectively.

There are interesting and potentially useful features in the mobility associated with uniaxial strain. In figure 4(*a*), we see that the red dashed line takes the form of a 'mobility well' instead of a 'mobility step', which is unique among the cases we explore. Intuitively, this line should appear as a 'reversal' of the blue dotted line (which represents the mobility results from [4] for biaxial strain), because in-plane biaxial tensile strain generates an out-of-plane uniaxial compressive strain (Poisson effect) if there is no constraint. In this sense, under [1 0 0] uniaxial tensile strain, the transverse mobility should stay at a low level and not increase. This would indeed be true if we could maintain the degeneracy between the [0 1 0] oriented Δ valleys and the [0 0 1] oriented Δ valleys. However, if these valleys become even slightly different in energy, the picture is dramatically changed. The mobility is sensitive to valley splitting even of the order of tens of meV. In our experiment, the substrate restricts relaxation of the silicon membrane along [0 1 0] directions and thus three sets of twofold degenerate valleys are obtained. The splitting between [0 1 0] valleys and [0 0 1] valleys is approximately 30 meV per 1% strain. At room temperature, the 30 meV difference will populate [0 0 1] valleys with three times as many electrons as [0 1 0] valleys. As a result, under [1 0 0] uniaxial tensile strain with confinement along the orthogonal direction, [0 0 1] valleys quickly dominate the transport with increasing tensile strain, and as a result the transverse mobility goes up. We can see that the transverse electron mobility, which is along [0 1 0] directions, is enhanced also when a compressive strain is applied along [1 0 0]. The electrons will prefer to occupy the [1 0 0] valleys because of their lower energy.

When comparing uniaxial tensile strain along [1 0 0] with the biaxial-tensile-strain case, we also need to change our earlier impression that [1 0 0] uniaxial strain has less enhancement than biaxial strain [10]. Here, as shown in figure 4(*a*), at lower strain (0–1%), uniaxial tensile strain along [1 0 0] has an effect on the longitudinal mobility improvement equal to tensile biaxial strain. At higher tensile strain (>1%), the [1 0 0] mobility actually exceeds the biaxial-tensile-strain mobility.

In figure 4(*b*), we see that there is no difference between the transverse and longitudinal mobilities (red dashed and black curves overlap). This result is not surprising, because, if we neglect the valley deformation, the effective masses along the [1 1 0] and [1 $\bar{1}$ 0] directions are always the same for each Δ valley. The in-plane mobility is in fact almost isotropic along any direction under this condition. The reason is that the valleys along [1 0 0] and [0 1 0] are always degenerate under [1 1 0] uniaxial tensile strain and thus the average in-plane effective mass becomes isotropic. Comparing with the mobility for biaxial tensile strain (dotted curve), the mobility

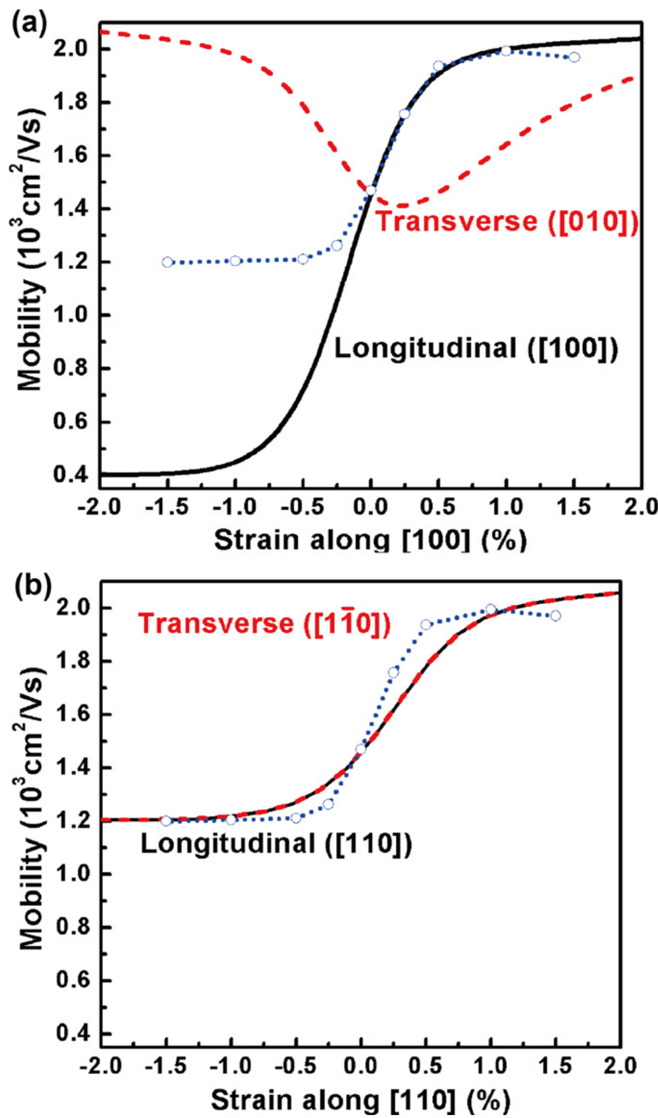

Figure 4. Calculated mobility as a function of uniaxial strain and comparison with our earlier work [4] for biaxial strain. (*a*) uniaxial strain along [1 0 0] and (*b*) uniaxial strain along [1 1 0]. The solid and dashed lines are for the longitudinal and transverse mobility. The dotted lines are for biaxial strain (from [4]).

for strain along [1 1 0] is lower at low strain (0–1%) but higher at higher strain (>1%). The general trend is consistent with earlier studies [20], but the crossing point is different (0.6% in [20] but 1% in this study).

In our calculation, we consider only the effect of valley splitting on electron mobility. Band warping, which we do not consider, induces an out-of-plane Δ_2 transverse effective-mass (m_t) change, and the mobility can be further enhanced [39]. Mobility enhancement induced by strain in MOSFETs is more complicated [20].

4. Conclusion

To summarize, we create uniaxial strain in Si nanomembranes that is similar to the commercial MOSFET strained-channel condition, i.e., the structure in the direction in plane but orthogonal to the stressing direction is confined. We modify the strain tensor to include the confined component instead of using the strain tensor appropriate to the free-boundary condition. Using this strain tensor, we extract the Δ and L_1 valley deformation potentials from our XAS data. They match the theoretical predictions. The deformation potential is also extracted for the L_3 valley, for which no theory or prior experiment of any sort exists. We find that under our experimental conditions, tensile uniaxial strain always enhances the in-plane electron mobility. For tensile strain in Si(0 0 1) along [1 0 0], the mobility enhancement is equal to that for biaxial strain at low strain but becomes greater at higher strain. In addition, our calculations show that compressive uniaxial strain along [1 0 0] can also be used to enhance the transverse mobility. Finally, uniaxial strain along the [1 1 0] direction, which tunes the in-plane mobility along all directions simultaneously, enhances the electron mobility in a manner similar to the effect of (0 0 1) biaxial strain.

Acknowledgments

This research is supported by DOE, Grant No DE-FG02-03ER46028 (FC, CE and MGL), by DOE Grant No DE-FG02-03ER46027 (FL) and by NSF/MRSEC Grant No DMR-0520527 (ZL and FH). The UW-Madison Synchrotron Radiation Center is supported by NSF Grant No DMR-0537588. FC was partially supported by the Chinese Scholar Council (CSC).

References

[1] Mohta N and Thompson S E 2005 *IEEE Circuit Devices Mag.* **21** 18
[2] Euaruksakul C, Li Z W, Zheng F, Himpsel F J, Ritz C S, Tanto B, Savage D E, Liu X S and Lagally M G 2008 *Phys. Rev. Lett.* **101** 147403
[3] Richard S, Aniel F, Fishman G and Cavassilas N 2003 *J. Appl. Phys.* **94** 1795
[4] Yu D, Zhang Y and Liu F 2008 *Phys. Rev.* B **78** 245204
[5] Takagi S I, Hoyt J L, Welser J J and Gibbons J F 1996 *J. Appl. Phys.* **80** 1567
[6] Sun Y, Sun G, Parthasarathy S and Thompson S E 2006 *Mater. Sci. Eng.* B **135** 179
[7] Sun G Y, Sun Y K, Nishida T K and Thompson S E 2007 *J. Appl. Phys.* **102** 084501
[8] Thompson S E *et al* 2004 *IEEE Trans. Electron Devices* **51** 1790
[9] Peterson R L, Hobart K D, Yin H, Kub F J and Sturm J C 2006 *J. Appl. Phys.* **100** 023537
[10] Yin H, Peterson R L, Hobart K D, Shieh S R, Duffy T S and Sturm J C 2005 *Appl. Phys. Lett.* **87** 061922
[11] Thompson S E *et al* 2004 *IEEE Electron Device Lett.* **25** 191
[12] Thompson S E, Sun G Y, Choi Y S and Nishida T 2006 *IEEE Trans. Electron Devices* **53** 1010
[13] Euaruksakul C *et al* 2009 *Phys. Rev.* B **80** 115323
[14] Sun Y, Thompson S E and Nishida T 2007 *J. Appl. Phys.* **101** 104503
[15] Park K H, Unuma T, Hirakawa K and Takagi S 2007 *Appl. Phys. Lett.* **91** 132118
[16] Thompson S E, Lim J S, Yang X and Nishida T 2006 *Appl. Phys. Lett.* **89** 073509
[17] Li M F, Zhao X S, Gu Z Q, Chen J X, Li Y J and Wang J Q 1991 *Phys. Rev.* B **43** 14040
[18] Tekippe V J, Chandras H, Ramdas A K and Fisher P 1972 *Phys. Rev.* B **6** 2348

[19] Murphy-Armando F, Fagas G and Greer J C *Nano Lett.* **10** 869
[20] Uchida K, Krishnamohan T, Saraswat K C and Nishi Y 2005 *IEEE Int. Electron Devices Meeting (Washington, DC)* vol 1089, p 135
[21] Li Y-H, Gong X G and Wei S-H 2006 *Phys. Rev.* B **73** 245206
[22] Fischetti M V and Laux S E 1996 *J. Appl. Phys.* **80** 2234
[23] van de Walle C G and Martin R M 1986 *Phys. Rev.* B **34** 5621
[24] van de Walle C G 1989 *Phys. Rev.* B **39** 1871
[25] Chelikowsky J R and Cohen M L 1976 *Phys. Rev.* B **14** 556
[26] Rideau D, Feraille M, Ciampolini L, Minondo M, Tavernier C, Jaouen H and Ghetti A 2006 *Phys. Rev.* B **74** 195208
[27] Roberts M M, Klein L J, Savage D E, Slinker K A, Friesen M, Celler G, Eriksson M A and Lagally M G 2006 *Nature Mater.* **5** 388
[28] Scott S A and Lagally M G 2007 *J. Phys. D: Appl. Phys.* **40** R75
[29] Cavallo F and Lagally M G 2010 *Soft Matter* **6** 439
[30] Arghavani R, Derhacobian N, Banthia V, Balseanu M, Ingle N, M'Saad H, Venkataraman S, Yieh E, Yuan Z, Xia L Q, Krivokapic Z, Aghoram U, MacWilliams K and Thompson S E 2007 *IEEE Trans. Electron Devices* **54** 362
[31] De Wolf I, Jian C and van Spengen W M 2001 *Opt. Laser Eng.* **36** 213
[32] Scott S A, Peng W N, Kiefer A M, Jiang H Q, Knezevic I, Savage D E, Eriksson M A and Lagally M G 2009 *ACS Nano* **3** 1683
[33] Lee P A, Citrin P H, Eisenberger P and Kincaid B M 1981 *Rev. Mod. Phys.* **53** 769
[34] Herring C and Vogt E 1956 *Phys. Rev.* **101** 944
[35] Bardeen J and Shockley W 1950 *Phys. Rev.* **80** 72
[36] Wortman J J and Evans R A 1965 *J. Appl. Phys.* **36** 153
[37] Yu P Y and Cardona D M 2001 *Fundamentals of Semiconductors—Physics and Materials Properties* 3rd edn (New York: Springer)
[38] Constancias C, Dalzotto B, Michallon P, Wallace J and Saib M 2010 *J. Vac. Sci. Technol.* B **28** 194
[39] Ungersboeck E, Dhar S, Karlowatz G, Kosina H and Selberherr S 2007 *J. Comput. Electron.* **6** 55
[40] Laude L D, Pollak F H and Cardona M 1971 *Phys. Rev.* B **3** 2623